Improvement in the Performance of Inverted 3D/2D Perovskite Solar Cells by Ambient Exposure

Yantao Wang,[1] Jingyang Lin,[1,2] Yanling He,[1] Yi Zhang,[1] Qiong Liang,[3] Fangzhou Liu,[1] Zhiwei Zhou,[4] Christopher C. S. Chan,[5] Gang Li,[3] Shien-Ping Feng,[4,6] Alan Man Ching Ng,[2] Kam Sing Wong,[5] Jasminka Popović,[7] Aleksandra B. Djurišić[1]*

[1]Dept. of Physics, Univ. of Hong Kong, Pokfulam Road, Hong Kong
E-mail: dalek@hku.hk
[2]Dept. of Physics, Southern University of Science and Technology, No. 1088, Xueyuan Rd., Shenzhen, 518055, Guangdong, PR China.
[3]Dept. of Electronic and Information Engineering, The Hong Kong Polytechnic University 11 Yuk Choi Rd, Hung Hom, Hong Kong
[4] Dept. of Mech. Eng, Univ. of Hong Kong, Pokfulam Road, Hong Kong
[5] Department of Physics, The Hong Kong University of Science and Technology, Clearwater Bay, Hong Kong.
[6]Department of Advanced Design and Systems Engineering, City University of Hong Kong, Kowloon, Hong Kong
[7]Division of Materials Physics, Ruđer Bošković Institute, Bijenička 54, Zagreb, Croatia

Abstract

Perovskite solar cells (PSCs) are known to be sensitive to the exposure to ambient humidity, which typically results in degradation and deterioration of performance, although positive effects of exposure to moisture have also been reported, due to recrystallization of the perovskite. To improve the PSCs stability, common approach is to use 3D/2D perovskite active layer, where 2D capping layer is prepared by spin-coating the bulky organic cation halide. Here we show that optimizing the exposure of the capping layer prepared by spin-coating phenylethylammonium iodide (PEAI) to ambient atmosphere results in substantial improvement of the PSC performance. Furthermore, we show that initial effects of PEAI treatment are dependent on the NiO_x/perovskite interface, but in all cases except at very high humidity (80-85% RH) optimized exposure to ambient results in improved performance. The variations in device performance with PEAI treatment and ambient exposure can be attributed to defect passivation and changes in the charge extraction due to energy level alignment at the interfaces. The best performing devices had passivation of NiO_x/perovskite interface and PEAI treatment of top surface followed by exposure to ambient atmosphere at RH of 40-45%, which resulted in the power conversion efficiency increase from 20.3% to 22.4%.

Keywords: Perovskite solar cells, ambient exposure, interfacial passivation, PEAI modification, 3D/2D perovskite

1. Introduction

Perovskite solar cells (PSCs) have attracted increased attention in recent years due to their high efficiency.[1-50] However, various instabilities under normal operating conditions (exposure to ambient air/moisture, illumination, elevated temperature, etc.) have been hindering the efforts in PSC commercialization.[1-3] Instability upon exposure to ambient/moisture is particularly pronounced in methylammonium (MA, CH_3NH_3) lead iodide, where water molecule reacts with the perovskite, which ultimately leads to a degradation into CH_3NH_2 gas, HI and PbI_2.[1-3] Composition engineering, such as using mixed cations and/or mixed halide anions to improve stability[1,2] and the use of 3D/2D perovskites[2] has been proposed to address this problem, but further advances are needed both in understanding the phenomena occurring in perovskite materials with more complex composition upon exposure to moisture, as well as stability improvements for practical applications.

The improvement in the performance (both efficiency and stability) of PSCs based on 3D/2D perovskites has been attributed to the passivation of defects at surface and grain boundaries, the hydrophobic nature of bulky organic cations of the 2D perovskite, and the modulation of charge transfer due to adjustment in energy level alignment across the interface.[2,4] Bulky organic cations can also inhibit ion migration and improve thermal stability, as well as enhance the film quality (crystallinity, orientation, etc.) of the perovskite film.[4] Different bulky organic cations have been reported for this purpose,[2-4,14,15,43] but phenethylammonium (PEA) remains among the most commonly used spacer cations for 3D/2D and quasi-2D perovskite films.[2-10,16-24,39,40,44,45-47,49] Its use has been demonstrated to improve stability of MA-based,[3] formamidinium (FA) - based,[2,4,7] and Cs-based perovskites,[40] as well as mixed composition perovskites.[4,5,8-10] In addition, it has been used as an additive to the perovskite to produce varying amounts and different 2D/quasi-2D

phases,[7,16,18,23,40] and to modify perovskite interfaces with electrode[9], top hole transport layer,[5,6,8,10,44] bottom hole transport layer,[20,39,45,49] top electron transport layer,[21,22,29,45,49] and both perovskite/charge transport layer interfaces.[19,49] Thus, it has been used both in inverted[20-22,29,39,45,49] and conventional,[5,6,8,10,44] architecture devices, but its use in inverted devices has been somewhat controversial, since contradictory results (worsening and improvement of the efficiency) have been reported in the literature when the PEAI is applied to the top interface of the perovskite. [20-22,29,45,49]

The 2D perovskite layer on the surface of the 3D layer is typically formed by surface treatment.[4] Surface treatment with PEAI in isopropanol (IPA) solution has been shown to lead to 2D perovskite formation due to the dissolution of MA^+ or FA^+ from the perovskite surface, facilitated by highly polar nature of IPA.[4,5] The formation of a 2D layer was also attributed to the reaction between PEAI and excess PbI_2, which is applicable to perovskite films prepared with solution stoichiometries with excess PbI_2.[10] It should be noted, however, that the PEAI treatment can also result in surface layer of PEAI rather than the formation of the 2D perovskite, and it has been proposed that PEAI is more beneficial than PEA_2PbI_4 for the device performance.[6] Furthermore, the effect of PEAI treatment on the top perovskite surface in an inverted perovskite structure is controversial, since both positive[21,22] and negative effects[19,21] on the device efficiency have been observed. This could occur due to differences in sample processing among different studies, since both higher and lower efficiency compared to device without PEAI could be obtained depending on the process used.[21] It was also found that the conversion of PEAI to PEA_2PbI_4 with elevated temperature is detrimental to the device performance,[6] and that devices with PEAI can exhibit improved performance after exposure to high humidity ambient,[16] but the effect of ambient exposure on the PEAI-treated perovskite has not been studied in detail and the relationship between the incorporation of PEAI and device efficiency and stability in inverted devices is not fully clear. However, the effect of moisture exposure on crystallinity of 3D perovskites has been studied

more comprehensively, and it has been reported that the moisture exposure can affect the crystallinity of 3D perovskites,[11,12] while trace water or ambient exposure can passivate the traps and suppress recombination and improve device performance.[13,25] In addition, MA/FA perovskite-based active layer treated with PEAI exhibited changes in the first several days which were attributed to reactions at interfaces.[5]

Thus, it is important to understand the nature of the layer formed on the surface and how it evolves over time, and how this affects the defect passivation and device performance. Therefore, we performed comprehensive characterization of the effect of the ambient exposure on PEAI-treated perovskite films as active layers of inverted PSCs for different ambient humidity levels. Since the mixed halide perovskites (MA-FA-Cs cations, I and Br anions)[42] are commonly used and result in excellent photovoltaic performance, we used the mixed composition perovskite for our investigation. We show that a significant improvement in device efficiency and stability can be achieved by optimized ambient exposure time for PEAI-treated perovskite films, which can be attributed to the moisture-induced recrystallization of the capping layer, resulting in improved defect passivation, improved charge extraction, and consequently improved device performance. In addition, we investigated the effect of PEAI-treatment on the device with and without surface modification of NiO_x/perovskite interface. We found that the PEAI treatment without ambient exposure can result in both worsening and improvement of the device performance, depending on the presence or absence of surface modification of NiO_x/perovskite interface, but the atmosphere exposure in all cases except very high ambient humidity resulted in further performance improvement. The differences are attributed to the differences in charge collection, caused by differences in energy level alignment across interfaces.

2. Results and Discussion

To investigate the effect of PEAI treatment and subsequent ambient exposure, we performed a comprehensive investigation of the samples without PEAI treatment and samples

treated with PEAI with different times of ambient exposure. The sample labels P_{no_0min}, P_{no_45min}, P_{0min}, P_{45min} denote perovskite film without ambient exposure, perovskite film exposed for 45 minutes in ambient at room temperature (60~65%RH unless specified otherwise), PEAI treated perovskite film without exposure, and PEAI treated perovskite film exposed to ambient for 45 minutes, respectively. The subscript in sample label indicates the ambient/moisture exposure time (MET). From SEM images (Supporting Information, **Figure S1**), we can observe that PEAI treatment results in an increase in grain sizes compared to the films without PEAI treatment, but no significant morphology difference can be observed for treated samples with and without ambient exposure. In addition, we can observe a change in morphology after PEAI treatment, namely the change in white appearance of grain edges (marked by circles), which can occur due to *in situ* passivation by PbI_2, and is expected to be present due to the non-stoichiometric ratio of the perovskite precursor for PbI_2 passivation.[27] It should be noted that it is not possible to conclusively identify a material just from SEM images, since contrast variations can also occur due to morphology/roughness differences and resulting charge accumulation at grain edges in less conductive materials. Since the samples that have been exposed to the ambient did not show obvious morphology differences, we also investigated their surface properties by contact angle (CA) measurements, and the obtained results are shown in **Figure S2**. The contact angle of untreated perovskite layer does not change significantly with ambient exposure (over the entire time contact angle stays in the range 42.2-42.7º, which is within sample-to-sample variation). In contrast, PEAI treatment without ambient exposure results in an increase in CA compared to untreated perovskite (53.4±1.0º) and the CA increases with increasing exposure time, becoming 57.1±1.4º for 15 min and 58.8±1.6º for 45 min MET. An increase in surface hydrophobicity is commonly observed after surface modification with organic halide compounds,[15] but the dependence of contact angle on the time of exposure to ambient has not been investigated. The change in

surface hydrophobicity implies a possible change in the surface composition, and it is expected to have positive effect on the device stability.

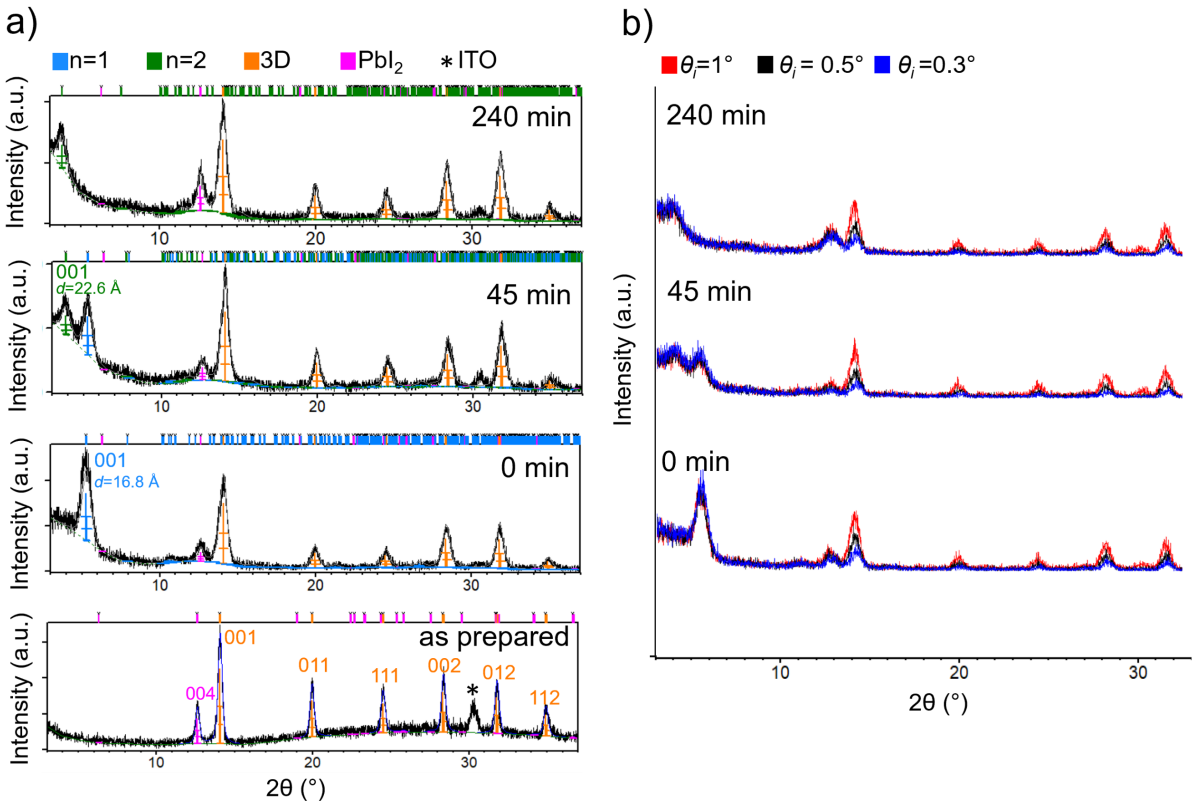

Figure 1. a) GI-XRD patterns (at incidence angle θ_i = 1°) of as-prepared sample and PEAI-treated samples exposed to ambient for 0 min, 45 min and 240 min. b) The effect of variable incidence angle θ_i (1°, 0.5° and 0.3°) on PEAI-treated samples exposed to ambient for 0 min, 45 min, and 240 min.

Figure 1a shows grazing incidence X-ray diffraction patterns (GI-XRD) at incidence angle θ_i = 1°. The as-prepared sample contains 3D $MAPbI_3$ and a small amount of hexagonal PbI_2. The 3D phase crystallizes in cubic P*m*-3*m* space group with the unit-cell parameter a = 6.292(1) Å which is in accordance with previous reports.[51,52] The addition of phenylethylammonium iodide induces the crystallization of 2D phase as evident by the prominent 001 line at d = 16.8 Å. Simultaneously with an appearance of 2D phase, we observe a slight decrease in the intensity of PbI_2 line in agreement with previous reports,[9,39] which implies that n = 1 phase is formed by the reaction between PEAI and excess lead

iodide.[10] While the n = 1 phase crystallizes immediately after the addition of PEAI, with further exposure to ambient conditions at t = 45 min, we observe an appearance of 001 line belonging to n = 2 at d = 22.6 Å that is accompanied by the pronounced decrease of 001 n = 1 reflection intensity, a small decrease of 3D reflection intensities and an increase of PbI_2 reflection intensity. The unit-cell parameter along the longest axis for both n=1 and n=2 are in accordance with those previously reported.[53,54] From the Figure 1b, showing diffraction data collected at variable incidence angles θ_i = 1°, 0.5 and 0.3 °, it is clearly evident that low-dimension 2D and quasi-2D phases crystallize at the surface of the 3D phase; as the grazing incidence angle decreases, the penetration depth of X-rays becomes reduced which leads to the attenuation of the intensities of crystalline phases coming from the interior of the film. With increased MET (240 min), only n = 2 phase can be observed and n = 1 phase disappears, while PbI_2 peak is more pronounced compared to 45 min of MET. The effects of ambient exposure have also been examined by XPS,[55,56] and the obtained results for oxygen, lead, and iodine peaks are shown in **Figures S3-S5** (no significant differences among samples were observed for other elements). Since the measurements have been done *ex situ* after transport to a different laboratory, additional effects of ambient exposure cannot be excluded, but since all the samples were subjected to the same transportation conditions it can still be informative to compare the effect of ambient exposure after PEAI treatment. We can observe that P_{45min} samples exhibit an increase in oxygen content (from 1.1 at% for P_{0min} to 4.6 at% for P_{45min}), while the oxygen content for P_{90min} decreases to below detection limit which could occur due to previously adsorbed oxygen/water on the surface reacting with the perovskite resulting in irreversible changes of composition. P_{45min} samples also have the lowest ratio of Pb^0 compared to Pb^{2+},[55] (4.1 % compared to 5.4% for P_{0min} and 5.5% for P_{90min}) which indicates protective effect of optimal time of ambient exposure against degradation (since the metallic Pb is the final degradation product resulting from the decomposition of PbI_2). We can also observe a shift in the iodide peak for 90 min ambient exposure, but this is difficult to interpret

since the XPS spectra differences between the perovskite and PbI_2 are small, and thus it can be more informative to look into Pb:I ratios.[56] From the I:Pb ratio which is higher than 4 but smaller than 7 we can conclude that both *n*=1 and *n*=2 PEA-based perovskite is present in the samples, and a small increase in I:Pb ratio (from 5.4 to 5.5) is in agreement with increasing contribution of *n*=2 phase observed in XRD with increasing time of ambient exposure. The samples exposed to ambient for 90 mins exhibit a drop in I:Pb ratio to 3.33 which is consistent with increasing PbI_2 content (from XRD measurements, the samples represent a mixture of PbI_2, 3D perovskite and quasi-2D n=2 perovskite).

Moisture-induced re-crystallization/reorientation has been previously observed in mixed halide 3D perovskite films, and it was found to be dependent on the amount of organic cation present on the film surface.[11] Significant improvements in the solar cell efficiency and stability was observed with excess organic cations, different from excess lead.[11] In 3D/2D perovskite devices, diffusion of PEAI into the grain boundaries[22] and changes in sample structure (simple 3D/2D vs. 3D/2D gradient mixture)[21] were found with thermal annealing and DMF addition, respectively. In both cases, there was a clear optimal condition (annealing time or DMF amount) which resulted in improved device performance. In our work, we observe the appearance of quasi-2D *n*=2 phase after exposure to moisture. Since we observe a concurrent increase in the presence of PbI_2 at the surface, a possible mechanism includes moisture induced degradation of the perovskite, followed by moisture-facilitated recrystallization and the formation of quasi-2D phase.

To investigate the effect of MET on device performance, P_{no}, P_{0min}, and PEAI with different MET were used as active layers in devices and obtained results from IV measurements are shown in **Figure 2**. The device structure and the chemical structures of relevant interface-modifying molecules are shown in **Figure S6, Supporting Information.** The device without PEAI modification showed average power conversion efficiency (PCE) of 16.5%, open circuit voltage V_{oc} of 1.0 V, short circuit current density Jsc of 21.8 mA/cm^2 and

fill factor (FF) of 76%. After PEAI surface modification, the average PCE decreased to ~14.5% which was mainly due to a significant drop of J_{sc} to ~17.9 mA/cm^2, despite increased V_{oc} and FF. This agrees with some of the literature reports,[19,45] and it can mainly be attributed to a decrease in short circuit current density.[45] This decrease likely occurs due to insulating nature of PEAI[21] and/or worsening of the charge collection at the top interface with ETL.[21,45] In inverted solar cells, PEAI has been proposed to be used for the modification of the bottom rather than the top interface,[45-47] although there have been reports where the PEA-based treatment of the top surface resulted in improved device performance.[29,49]

For devices based on ambient exposed PEAI-treated perovskite, J_{sc} increased to ~20.6 mA/cm^2 after 15-minute exposure and reached its maximum around 22 mA/cm^2 after 45-minute exposure, while V_{oc} and FF also increased. However, for MET longer than 45 min., FF starts to decrease, followed by J_{sc} decrease after 90 min. The champion cell obtained for P_{45min} obtained a 20.13% PCE by reverse scan and 20.18% PCE by forward scan. EQE plots and I-V curves for champion devices are shown in **Figure S7**, Supplementary Information. Good agreement is obtained between measured J_{sc} and estimated values from integrated EQE curves. Thus, we can observe that MET not only leads to structure changes but also significant device performance differences. While in conventional devices the presence of n>1 phase was found to be detrimental to the hole transfer across the perovskite/HTL interface,[24] we find that the presence of mixed phases n=1 and n=2 at the top interface is actually beneficial for the device performance. This could be due to improvement in charge transport, since it has been proposed that phase-pure quasi-2D PEA_2PbI_4 layer oriented parallel to the substrate strongly retarded the charge transport.[47] However, it is necessary to carefully examine the reasons responsible for the observed improvements in the performance, since the improvement in charge transport for n=2 phase compared to n=1 phase is not expected to be very significant.

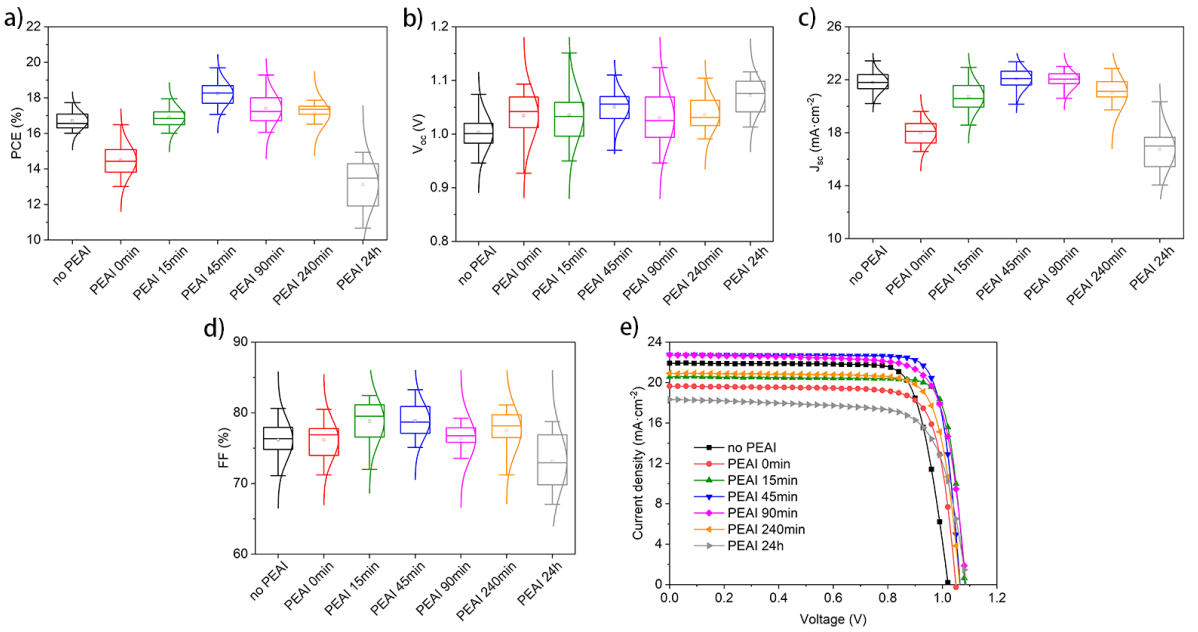

Figure 2. The performance distribution graphs of a) PCE, b) V_{oc}, c) J_{sc} and d) FF, as well as e) Champion IV curves for PSCs based on P_{no}, P_{0min}, and PEAI exposed for different time periods. The red spots in the graph a~d) refer to average values obtained for 20 devices.

In addition to solar cell performance, we investigated the effect of PEAI treatment and ambient exposure on the device stability, and the resulting PCE vs. time curves under maximum power point tracking (MPPT) of unencapsulated devices in ambient (tests performed until 80% of initial PCE is reached) are shown in **Figure 3.** The P_{no} device showed a fast degradation with T_{80} of 4.5 h, while both PEAI-treated devices exhibited improved lifetime as expected, since PEAI treatment is known to enhance the stability of the devices in ambient due to its hydrophobic properties,[10,19] and it is expected to also result in reduced ion migration since it can passivate defects.[10] The obtained T_{80} times were 52 h for P_{0min} and 64 h for P_{45min}. We can observe similar Secondary ion mass spectroscopy (SIMS) profiles for initial P_{0min} and P_{45min} based devices and corresponding devices which were degraded to 80% of initial efficiency, as shown in **Figure S8**, indicating that both PEAI-modified devices do not exhibit obvious evidence of ion migration in the early stages of degradation of performance. The P_{0min} device showed an increase in PCE in the first 10 h of ambient

exposure, mainly due to increased J_{sc} consistent with samples with increased MET, and a previous literature report on increased efficiency of PEAI-treated devices with ambient exposure.[16] The device then exhibited 25 h of steady output, followed by a decrease in PCE. P_{45min} device exhibited steady performance, followed by decrease in performance, which occurred at a later time compared to P_{0min} device, indicating enhanced stability. The eventual deterioration of the performance likely occurs due to eventual degradation of the perovskite layer, since we can observe an increase in PbI_2 content with increased time of ambient exposure for the perovskite films, as shown in Figure 1.

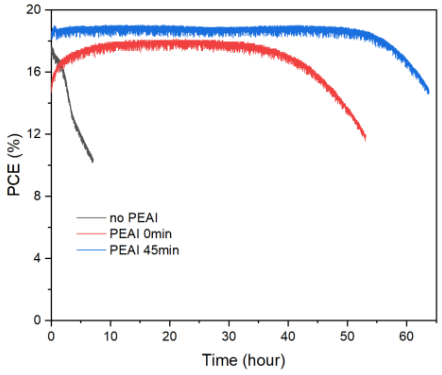

Figure 3. The operating stability test for P_{no}, P_{0min}, P_{45min} based devices at MPP under AM1.5 light illumination in ambient without encapsulation.

The effect of ambient exposure on device performance was dependent on the ambient humidity level, but in all cases except the highest humidity level considered (80-85%), the improvement in performance was obtained after ambient exposure, as shown in **Figure S9** and **Table S1**. We can observe that at low relative humidity (30-35%) performance continues to improve to 90 min of exposure, while at high RH (80-85%) performance deteriorates with ambient exposure. For the RH levels of 45-50% and 60-65%, optimal performance is observed for 45 min of ambient exposure, and the devices exposed to ambient at RH of 60-65% give overall the best performance. In all cases, the PEAI treatment initially worsens performance (P_{0min} samples) compared to the devices without PEAI (P_{no} samples).

To understand the correlation between the structural changes and the optical properties of the material, steady state photoluminescence (PL) was measured for PEAI/perovskite/glass substrate samples without HTL, and obtained results are shown in **Figure 4a**. PL intensity enhancement after PEAI treatment is consistent with previous reports,[5,8,21] and it indicates suppressed nonradiative recombination due to defect passivation and overall improved film quality.[6,12,21] The PL intensity first increases then decreases with increasing MET (optimal humidity level of 60-65% RH), consistent with the trends observed in device performance. A small red shift of PL peak position from 760.5 nm to 770.5 nm was also observed with increased MET, which is consistent with Ref.[11] but different from the behavior observed in all-inorganic perovskites.[12]

This is consistent with observed changes in XRD demonstrating recrystallization of 3D/2D perovskite to form quasi-2D phases. To obtain further insight into the device performance dependence on MET, we performed comprehensive electrical characterization of the devices. The space charge limited current (SCLC) measurements were carried out on the single electron carrier devices with configuration of ITO/SnO_2/perovskite/P_{no} or P_{0min} or P_{45min}/PCBM/BCP/Ag as shown in **Figure 4b**. The trap density N_t can be determined according to equation 1:[15,19,33-36]

$$N_t = \frac{2\varepsilon\varepsilon_0 V_{TFL}}{eL^2} \quad (1)$$

where ε, ε_0, V_{TFL}, L and e represent the relative dielectric constant (62.23 [34]), vacuum permittivity (8.8542×10^{-14} F/cm), trap filling limited voltage, the thickness of the perovskite film (~425 nm) and the elementary charge (1.602×10^{-19} C), respectively. V_{TFL} was determined from the measured I-V curves. Distinct regions can be observed in the $I\sim V^n$ dependences, with ohmic regime at low voltage corresponding to n=1, followed by trap filling regime (if any) with high slope n>2, and finally space charge limited current (SCLC) regime with n=2.[57,58]

Here we determined V_{TFL} from the intersection of the tangents to the ohmic and trap filled regimes, respectively, as commonly applied procedure.[20,58] While the absolute value of trap density can vary depending on the method of V_{TFL} determination,[57] relative comparison of defect density would not be affected, especially since the slope in the trap filled regime is high. It can be observed that the V_{TFL} decreased significantly from 0.371 V for P_{no} based device to 0.245 V and 0.212 V for P_{0min} and P_{45min} based devices, respectively. The electron trap density of P_{45min} based single carrier device is calculated to be 3.59×10^{15} cm^{-3}, which is lower than that of P_{0min} (4.11×10^{15} cm^{-3}) and P_{no} (6.31×10^{15} cm^{-3}) based sample, indicating the improved perovskite film quality[34] after moisture exposure. The reduction in the trap density after surface treatment with bulky organic ammonium halide compared to untreated 3D perovskite has been observed for different cations and can be attributed to the defect passivation of the organic cation.[4,15,16] The exposure to moisture further reduces defect density, likely due to observed recrystallization and/or diffusion of PEA into the grain boundaries. To obtain further insight into the effects of PEAI surface modification and MET, the Mott-Schottky (MS) measurement was conducted to the P_{no}, P_{0min}, P_{45min} based devices, with AC excitation amplitude of 20 mV at constant frequency of 10 kHz.[36] The capacitive behavior of the perovskite solar cells is complex, with different contributions dominating at different frequency ranges.[59] In our samples, capacitance plateau corresponding to the depletion layer capacitance[59] was typically observed in the frequency range ~4kHz-100kHz, hence we have selected 10kHz as measurement frequency. The relationship between the capacitance and voltage is described by the Mott-Schottky equation as follows:[37]

$$C^{-2} = \frac{2(V_{bi}-V)}{A^2 q\varepsilon\varepsilon_0 N} \quad (2)$$

where V_{bi} stands for the built-in potential, V the applied voltage, A device active surface (0.14 cm^2), and N the doping density of perovskite, and the obtained C^{-2} *vs*. V plots are shown in **Figure 5c**, where the V_{bi} values were deduced by the intersection with the x-axis. Compared

to the V_{bi} of P_{no} (0.813 V) and P_{0min} (0.849 V) based device, the P_{45min} based device had a higher V_{bi} of 0.872 V. The increased V_{bi} indicates larger driving force for photo-generated charge carrier separation, transport and extraction, as well as less screening effect where charge carriers are trapped due to interface trap states,[37] which is consistent with the J-V curves in Figure 4. The calculated defect densities are 3.867×10^{15} cm^{-3}, 6.481×10^{15} cm^{-3}, 6.756×10^{15} cm^{-3} for P_{45min}, P_{0min}, and P_{no}, in agreement with passivating effects of PEAI treatment and optimal MET based on SCLC measurements. Finally, to examine the recombination in the devices, we conducted measurements of the V_{oc} dependence on the light power density, as shown in **Figure 4d**, to determine the presence of defect-assisted or monomolecular Shockley-Read-Hall (SRH) recombination. The ideality factor n_{ID} has a relationship with V_{oc} and light intensity I according to the following equation:

$$qV_{oc} = E_g + n_{ID}kTln(\frac{I}{I_0}) \quad (3)$$

where q stands for the elementary charge, k the Boltzmann constant, T the absolute temperature, E_g the band gap of perovskite.[5,19] It is known that n_{ID} value higher than 1 reflects the occurrence of defect-assisted recombination in the PSCs.[5,36,37] The n_{ID} values closer to 1 suggest reduced contribution of SRH recombination, in agreement with reduced trap densities determined from SCLC measurements[14,30-32,36] and increased fill factor. The decreased n_{ID} implies that the trap-assisted recombination was reduced by PEAI passivation and further exposure, as the obtained values decrease from n_{ID}=1.22 for P_{no} to n_{ID}=1.19 for $P_{0\ min}$ and finally to n_{ID}=1.08 for $P_{45\ min}$ samples.

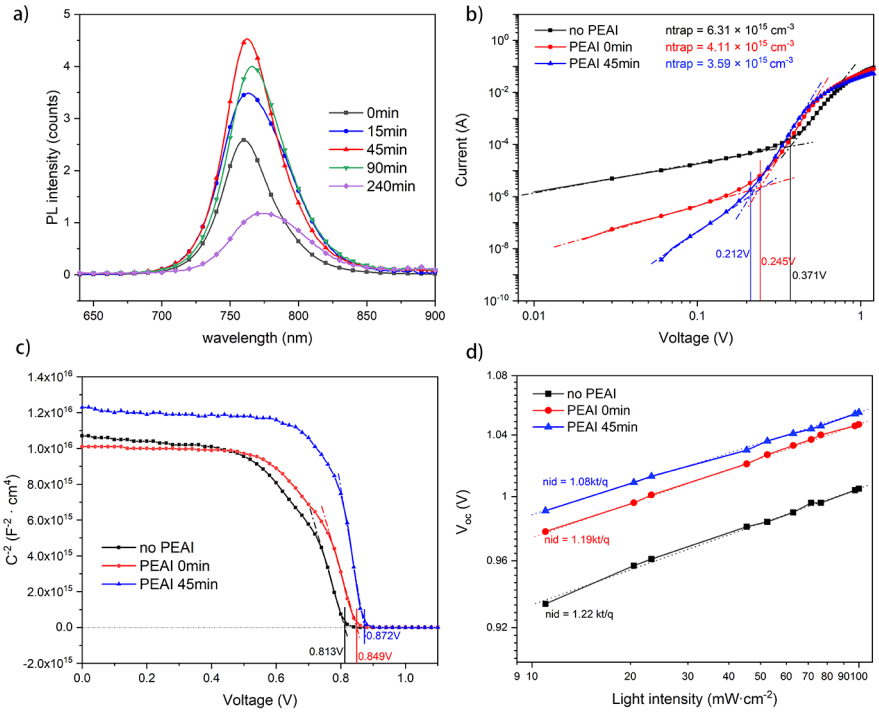

Figure 4. a) PL spectra and b) SCLC, c) MS and d) V_{oc} vs light intensity curves for P_{no}, P_{0min}, P_{45min} based devices.

To further clarify the reasons for the observed performance differences, more specifically to understand why the PEAI treatment initially worsens the J_{sc} and PCE despite defect passivation by PEAI treatment, we performed UPS measurements[60,61] to determine the positions of the energy levels and assess the implications of energy level alignment on the charge collection. Obtained results are shown in **Figure 5**, where the energy level alignment after each successive layer has been plotted with common Fermi level, since in UPS the measured work function is a combination of Fermi level and vacuum level[60] and it is known that there is charge transfer at perovskite interfaces which can lead to dipole moments and vacuum level shifts.[61] LUMO levels have been added based on the bandgap values determined from absorption spectra for our 3D perovskite and reported literature values for NiO_x, PCBM, and PEA-based n=1 perovskite.[20,62]

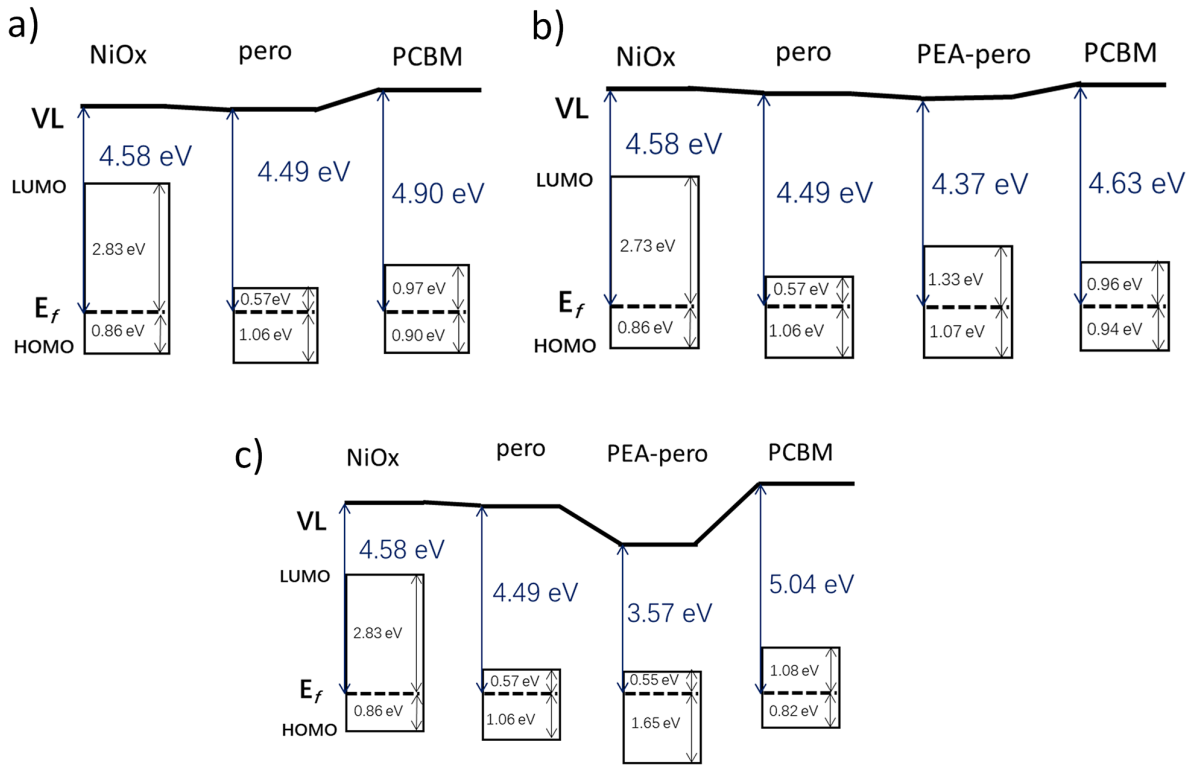

Figure 5. Energy level alignments in different devices a) P_{no} b) $P_{0\ min}$ and c) P_{45} min.

We can observe that PEAI treatment without ambient exposure results in an energy level alignment which introduces a barrier for electron collection, which is consistent with observed significant decrease in J_{sc} and consequently PCE for $P_{0\ min}$ devices. For the samples exposed to ambient, we can observe a significant downshift of the vacuum level and HOMO/valence band maximum level, resulting in the removal of barrier for electron collection, consistent with the observed increase in the J_{sc} and the corresponding increase in PCE. It is known that the energy levels determined by UPS can shift with the sample exposure to ambient.[61,63] The vacuum level shift upon exposure was found to increase with time, and the downshift of the vacuum level and valence band maximum/HOMO level was found with exposure to water.[63] Thus, the observed shifts in energy level can be attributed to water exposure causing interface dipoles, with observed recrystallization of PEA-based perovskite as additional contributing factor. From the TRPL data (**Supporting Information, Figure S10** and **Table S2**), we can observe that all the data can be fitted with biexponential decay curves.[20,64,65] The fast decay

time in perovskite films is commonly attributed to surface recombination (and it is also indicative of charge extraction in perovskite films with charge transport layers), while slow decay time is attributed to bulk recombination.[20,64,65] PEAI treatment was previously reported to result in an increased average decay time attributed to decreased nonradiative recombination in 2D/3D perovskite films, while the faster hole extraction was observed in 2D-3D/hole transport layer samples compared to 3D perovskite,[10 consistent with previous findings. The increased lifetime is attributed to both defect passivation and less efficient charge collection, in agreement with other characterization results. Upon ambient exposure, a significant decrease of both fast and slow decay times is observed for the PEAI samples ($P_{0\ min}$ compared to $P_{45\ min}$). A more efficient charge transfer can result in a significant decrease of both fast and slow decay time,[65] while efficient defect passivation can result in significant increases in decay time despite efficient charge extraction,[66] indicating that both fast and slow decay are affected by both charge transfer and trap passivation. Therefore, TRPL data should be interpreted with care together with other characterization techniques. From Figure 4a, the PL of the film exposed for 45 minute is much higher than that of the $P_{0\ min}$ sample, we therefore attribute its decreased lifetime in the structures in Figure S10 to a more efficient charge transfer.[65].

PEAI modification was previously reported to result in increased PL intensity for bare films, and more efficient quenching for 2D/3D/PCBM films compared to 3D/PCBM,[20] indicating that not only trap passivation but an improvement in charge extraction is possible with PEAI treatment in inverted architecture.[20] This is in agreement with reported improved solar cell performance of inverted devices with PEAI,[20,29,49] and different from the behavior observed here. Since the reduction in the efficiency with PEAI treatment without ambient exposure can be clearly attributed to the unfavorable energy level alignment, and since the devices reporting improvement used NiO_x hole transport layers prepared by different methods[20,29] compared to this work, we investigated the devices with NiO_x surface modification in an

attempt to alter the energy level alignment. We have used [2-(9H-carbazol-9-yl)ethyl]phosphonic acid (2PACz) to modify NiO_x surface, since these molecules have been shown to facilitate charge collection in inverted perovskite solar cells.[66] The performance of the devices with 2PACz modification for 3D perovskite (P_{no}), and 3D/2D perovskite with different times of ambient exposure ($P_{0\ min}$, $P_{45\ min}$, $P_{90\ min}$) and different relative humidity levels is shown in **Figure S11** and **Table S3, Supporting Information**.

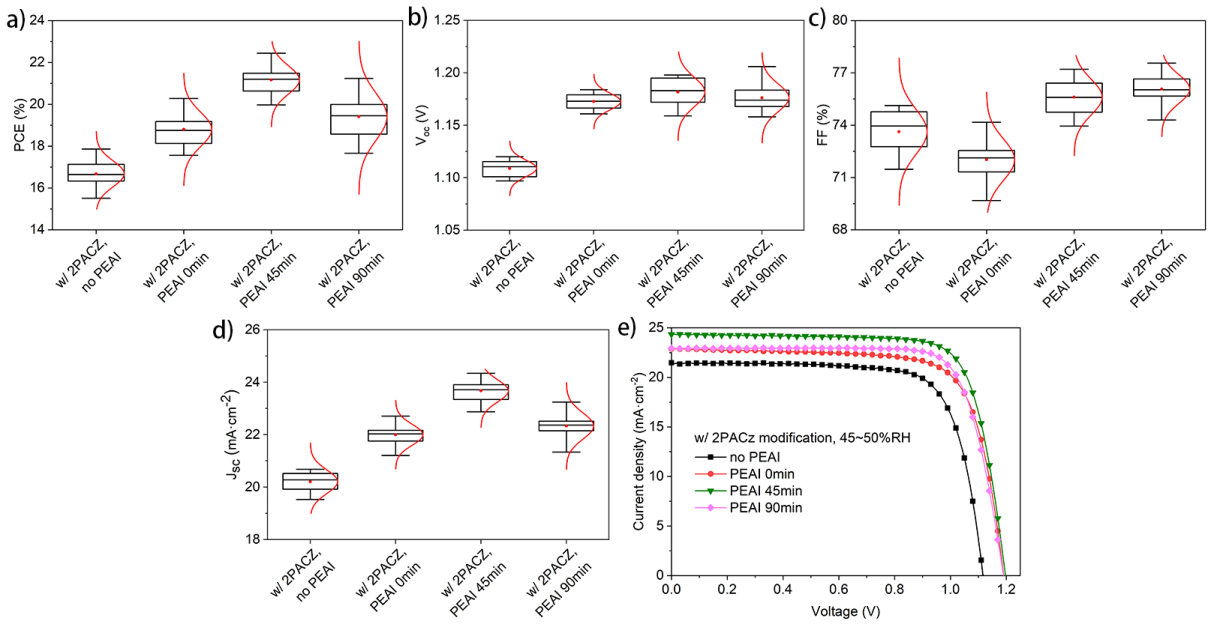

Figure 6. The performance distribution graphs of a) PCE, b) V_{oc}, c) J_{sc} and d) FF, as well as e) Champion IV curves for PSCs based on P_{no}, P_{0min}, and PEAI exposed for different time periods. The red spots in the graph a~d) refer to average values obtained for 20 devices.

We can observe that in this case PEAI treatment results in an improvement of the device performance compared to 3D perovskite (arising from improved J_{sc} and V_{oc}), different from devices without 2PACz. In addition, the dependence of performance on the relative humidity is different as well. Performance improvements are observed only for the condition 45-50% RH, where a significant increase in all performance parameters, as shown in **Figure 6**, is observed. To investigate the reasons for the observed differences, UPS measurements have been performed, and the obtained results are shown in **Figure 7**. For 3D perovskite devices,

we can observe that electron collection barrier increases with 2PACz compared to no 2PACz, consistent with slightly lower J_{sc}. However, V_{oc} is higher in devices with 2PACz, consistent with lower recombination losses and longer slow decay time in TRPL, so that overall slightly higher efficiency is obtained. This is in agreement with a previous report on defect passivation in perovskite prepared on 2PACz, which was attributed to chemical compatibility between carbazole and perovskite.[66] With PEAI treatment, we can observe a significant increase in J_{sc} and a small increase in V_{oc}, which can be attributed to an improvement in the electron collection due to more favorable energy alignment (Figure 7b). We also observe a significant increase in PL decay times, which is consistent with a previous report where even higher carrier lifetime compared to films on quartz (no charge transfer) was observed for 2PACz.[65] For 45 min of ambient exposure, all device parameters increase significantly indicating lower recombination losses as well as improved charge extraction, resulting in the best efficiency of 22.45%, significantly improved compared to devices without ambient exposure (20.28%) and devices without PEAI (17.98%). In addition, with 45 min ambient exposure to ambient the PL decay time decreases, consistent with more efficient charge collection due to the downshift of the LUMO/conduction band minimum of the 2D/quasi-2D surface layer.

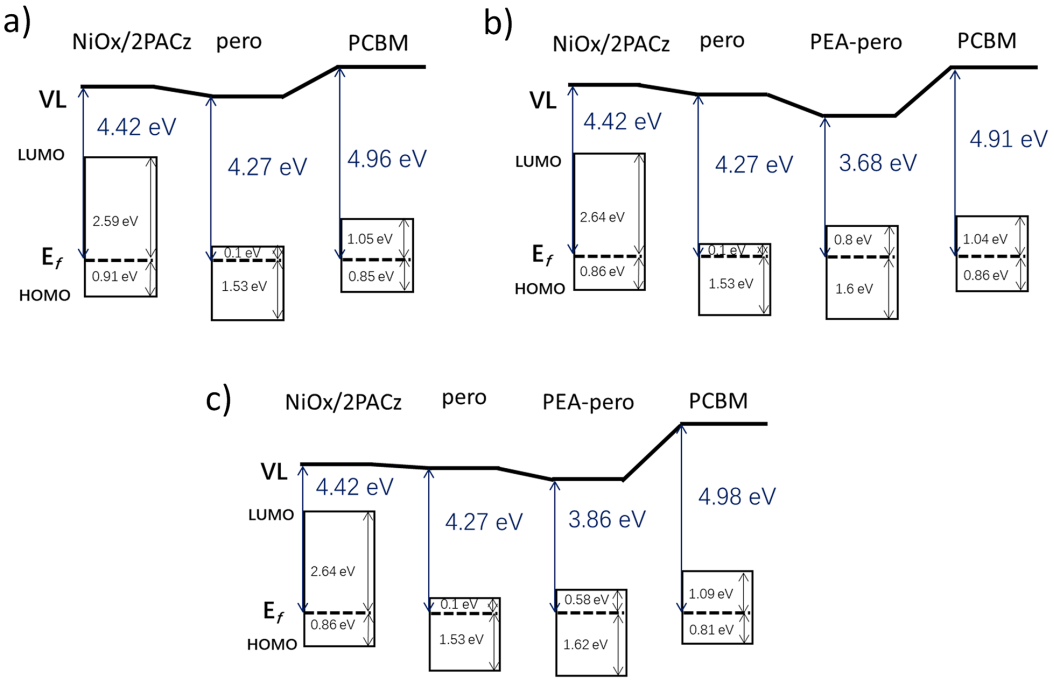

Figure 7. Energy level alignments in different devices with 2PACz for a) P_{no} b) $P_{0\ min}$ and c) P_{45} min.

Thus, the observed changes in the device performance with and without PEAI, as well as with ambient exposure after PEAI treatment, can be attributed to the changes in the energy level alignment which affect charge collection from the devices. We also clearly demonstrate that the use of interfacial layers at buried interfaces (NiO_x/2PACz) can affect the energy level alignment in the entire device, which can occur due to charge transfer and interface dipole formation resulting in Fermi level pinning.[61]

3. Conclusion

We investigated the effect of ambient atmosphere exposure on the properties of 3D/2D perovskite films and their device performance. We observed that 3D/2D structure which initially forms upon spincoating PEAI transforms to a mixture of n = 1 and n = 2 phases with increased time of ambient exposure, until finally only n = 2 phase is observed and PbI_2 content increases again. More importantly, exposure to ambient humidity results in a significant shift in the energy level alignment due to a large vacuum level shift, lowering the barrier for the electron collection due to unfavorable alignment at 3D/2D interface without ambient exposure. There is an optimal time of atmosphere exposure (45 min) and optimal relative humidity level, where we can obtain the advantages of improved charge collection and reduced recombination, without worsening of the performance due to perovskite decomposition with further increase of ambient exposure. Furthermore, the energy level alignment at 3D/2D interface is also affected by the energy level alignment at NiO_x/3D interface. Interfacial modification with 2PACz results in increased carrier lifetime as well as Fermi level pinning near the LUMO of the perovskite, which results in a more favorable energy level alignment for electron collection at 3D/2D interface. Therefore, the literature contradictions on whether the PEAI treatment leads to improved efficiency in inverted

perovskite solar cells likely originate in differences in the energy level alignment at the hole transport layer/perovskite interface. The use of hole transport layers or interfacial layers leading to charge transfer and Fermi level pinning could thus enable reliable and effective use of 2D perovskite modifications of the top perovskite surface in inverted devices, not only conventional ones.

4. Experimental Details

Materials

N,N-Dimethylformamide (DMF), dimethyl sulfoxide (DMSO), iso-propanol (IPA), and cesium iodide were purchased from Alfa Aesar, chlorobenzene (CB) and ethylenediamine (EDA) from Sigma-Aldrich, [2-(9H-Carbazol-9-yl)ethyl]phosphonic Acid (2PACz), lead iodide (PbI_2) and lead bromide ($PbBr_2$) from TCI, formamidinium iodide (FAI) and methylammonium bromide (MABr), phenethylammonium iodide (PEAI) from GreatCell Solar, (6,6)-Phenyl C61 butyric acid methyl ester (PCBM) and bathocuproine (BCP) from Lumtec, $Ni(NO_3)_2{\cdot}6H_2O$ from International Laboratory, and ethylene glycol (EG) from Dickmann. All the chemicals are used as received.

Preparation of precursors

The preparation of NiO_x sol-gel precursor followed the reported procedure in Ref.[41] Briefly, 1.454 g $Ni(NO_3)_2{\cdot}6H_2O$ was dissolved in 5ml EG, then 335 µl EDA was added to the solution at room temperature with mild stirring for 4 h. The perovskite precursor preparation followed the procedures reported in Ref.[42] Briefly, 800 µl DMF and 200 µl DMSO were added into the vial with 18.2 mg CsI, 22.4 mg MABr, 172 mg FAI, 73.4 mg $PbBr_2$, 507.1 mg PbI_2 with vigorous stirring at 65°C for 60 min then cooled down to room temperature. All the precursor solutions were used after filtering by 0.22 µm PTFE filters.

Device fabrication

25×25 mm^2 ITO substrates were ultrasonically cleaned with detergent solution, DI water, acetone, and IPA sequentially for 15 min for each step, followed by oxygen plasma treatment

at 10 V bias for 2 min. NiO_x precursor was then spin coated on the freshly treated ITO at 5000 rpm for 50 s, followed by 300 ºC annealing for 50 min. in ambient. NiO_x substrates were transferred to the glovebox immediately once cooled down to 80ºC. For 2PACz modified devices, 70 µl 2PACz solution in IPA (0.75 mg/ml) was statically spin-coated on NiO_x substrate at 4000 rpm for 35 s, then annealed at 120ºC for 10 min and cooled down to room temperature. To prepare perovskite film, 55 µl of perovskite precursor solution was spread on the surface and spin-coated at 4000 rpm for 35 s, with 350 µl CB dripping added 10 s after the start of spin-coating, followed by 110 ºC annealing for 20 min. After cooling down for 15 min, 70 µl PEAI solution (2 mg/ml in IPA) was dynamically spin-coated at 5000 rpm for 35 s, followed by annealing at 100ºC for 10 min. To expose the samples to ambient air at different relative humidities, the samples were transferred to a home-made controlled humidity environment consisting of a vacuum oven, water-filled Petri dishes, compressed air cylinder providing dry air, and a Bluetooth enabled hygrometer. For control devices, ambient exposure was omitted. After exposure, the substrates were moved back to the glovebox for PCBM layer dynamic spin coating (40 mg/ml in CB, 5000 rpm 35 s). After annealing for 10 min at 100 ºC and cooling down, 70 µl BCP saturated solution in IPA was deposited on PCBM layer at 4000 rpm for 30 s. Finally, the 80 nm Ag electrode was deposited through a shadow mask by a thermal evaporator at the rate of 0.1 Å/s for the initial 10 nm, and 0.5 Å/s for the remaining thickness.

Characterization

In all characterizations, samples were kept in argon before the measurement, and unwanted ambient exposure was minimized in sample handling. The contact angle tests were measured by a 100SB Sindatek contact angle meter and a Magic drop software was used to calculate contact angle results. 5 µl water drop was dripped and dwelled on all samples for 5 s to eliminate errors. The surface and cross-section morphology images were characterized by

scanning electron microscopy using a Hitachi S4800 FEG-SEM. Mott Schottky plots were obtained with a CHI660C electrochemical workstation. GIXRD data were measured using a Rigaku Smartlab 9KW X-ray Diffractometer. X-ray photoelectron spectra (XPS) were obtained using an ESCALAB 250xi from Thermo Fisher XPS. The C1s binding energy of 284.8 eV was used as energy reference. The UPS spectra were measured using the same instrument, and a helium discharge lamp with energies of 21.22 eV was used to excite electrons from the valence band. The work function was determined by measuring the width of the emitted electrons (W) from the cutoff of the secondary electrons up to the Fermi edge and subtracting W from the energy of the incident UV light (21.22 eV). The work function is strongly affected by the condition of the surface and the energy band alignment at the interface of the semiconductor. These changes are a result of the formation of dipole moments at the surface/interface (the presence of a vacuum shift), which changes the work function. A bias voltage of 10 V was applied during UPS measurements to obtain the true energy cutoff of secondary electrons. Au was measured as a reference for the Fermi level. The HOMO/valence band maximum (VBM) level was determined by the first ionization energy. In a semiconductor, the ionization energy is the difference between HOMO (VBM) and the vacuum level. The optical band gap of the semiconductor was used to determine the LUMO/conduction band minimum (CBM) level.

Time resolved photoluminescence was carried out with excitation provided by a 640 nm picosecond diode laser (Edinburgh instruments) operating at 1MHz with an intensity of ~15 nJ cm^{-2} on the substrate side of the sample. The photoluminescence was collected and sent into a monochromator (Acton SpectraPro 275) where the PL center wavelength was sent into a photon counter at the exit port. Time correlated single photon counting was carried out using a Becker and Hickl system (SPC150). Steady state PL measurements were performed with a CVI Melles Griot LC500 HeCd laser as an excitation source. UV-Vis spectra were carried out with a Cary 60 UV-Vis spectrophotometer.

I-V measurements were carried out using a Keithley 2400 Source Measure Unit in ambient (22 ºC, 60~65% RH). The simulated solar illumination was provided by ABET Sun 2000 solar simulator with 100 mW/cm^2 illumination intensity and AM1.5G spectrum, and the light intensity is calibrated by Enli PVM silicon standard reference cell every time before I-V test. The devices are measured both in reverse scan (1.2V to -0.2V) and forward scan (-0.2V to 1.2V) with a step size of 10 mV and a delay time of 10 ms. The long term MPP operating stability test is conducted for unencapsulated devices under continuous AM1.5G illumination in ambient environment (60~65% RH, 33~35ºC for substrate surface temperature). The device active area was 0.14 cm^2 (0.35cm × 0.40cm), and a mask with aperture area of 0.08 cm^2 was used to prevent any scattered light to contribute to the photocurrent.

Supporting Information

Supporting Information is available from the Wiley Online Library.

Author Contribution Statement

YT Wang and A B. Djurišić conceived the idea and designed the experiments. A B. Djurišić and A. M. C. Ng supervised the project. YT Wang prepared and characterized the solar cells. JY Lin, Q Liang, FZ Liu, Z Zhou, G Li, and SP Feng helped perform the related film and device measurements. YL He and AMC Ng performed XPS and UPS measurements and analyzed the data, while CCS Chan and KS Wong measured analyzed TRPL data. J Popović analyzed XRD data. YT Wang, J Popović, and A B. Djurišić composed and revised the paper. All authors discussed and analysed the results and provided input to the manuscript.

Acknowledgements

This work is supported by RGC CRF grant C5037-18G and C7018-20G, Seed Funding for Strategic Interdisciplinary Research Scheme of the University of Hong Kong and Shenzhen Science and Technology Commission Project No. JCYJ20170818141216288. Support from

project PZS-2019-02-2068 financed by the "Research Cooperability" Program of the Croatian Science Foundation funded by the European Union from the European Social Fund under the Operational Programme Efficient Human Resources 2014-2020 is also acknowledged. The authors thank Dr. S. Ruan for FTIR measurement.

Received: ((will be filled in by the editorial staff))

Revised: ((will be filled in by the editorial staff))

Published online: ((will be filled in by the editorial staff))

References:

[1] Q. Wali, F. J. Iftikhar, M. E. Khan, A. Ullah, Y. Iqbal, R. Jose, *Org. Electron.* **2020**, *78*, 105590.

[2] S. P. Dunfield, L. Bliss, F. Zhang, J. M. Luther, K. Zhu, M. F. A. M. van Hest, M. O. Reese, J. J. Berry, *Adv. Energy Mater*. **2020**, *10*, 1904054.

[3] P. Roy, N. K. Sinha, S. Tiwari, A. Khare, *Sol. Energy* **2020**, *198*, 665.

[4] M. A. Mahmud, T. Duong, J. Peng, Y. L. Wu, H. P. Shen, D. Walter, H. T. Nguyen, N. Mozaffari, G. D. Tabi, K. R. Catchpole, K. J. Weber, T. P. White, *Adv. Funct. Mater.* **2021**, 202009164.

[5] T. Zhu, D. M. Zheng, J. W. Liu, L. Coolen, T. Pauporté, *ACS Appl. Mater. Interfaces* **2020**, *12*, 37197.

[6] Q Jiang, Y. Zhao, X. W. Zhang, X. L. Yang, Y. Chen, Z. M. Chu, Q F. Ye, X. X. Li, Z. G. Yin, J. B. You, *Nat. Photonics* **2019**, *13*, 460.

[7] N. Li, Z. L. Zhu, C. C. Chueh, H. B. Liu, B. Peng, A. Petrone, X. S. Li, L. D. Wang, A. K.Y. Jen, *Adv. Energy Mater*. **2017**, *7*, 1601307.

[8] H. S. Yoo, N. G. Park, *Sol. Energy Mater. Sol. Cells* **2018**, *179*, 57.

[9] K. S. Lee, J. W. Kim, H. J. Yu, J. W. Lee, C. M. Yoon, S. K. Kim, J. S. Jang, *J. Mater. Chem. A* **2018**, *6*, 24560.

[10] P. Chen, Y. Bai, S. C. Wang, M. Q. Lyu, J. H. Yun, L. Z. Wang, *Adv. Funct. Mater.* **2018**, *28*, 1706923.

[11] J. Hidalgo, C. A. R. Perini, A.-F. Castro-Mendez, D. Jones, H. Köbler, B. Lai, R. P. Li, S. J. Sun, A. Abate, J.-P. Correa-Baena, *ACS Energy Lett.* **2020**, *5*, 3526.

[12] Z. Z. Li, X. L. Liu, J. Xu, Y. J. Liao, H. Zhao, B. Zhang, S. Z. F. Liu, J. X. Yao, *J. Phys. Chem. Lett.* **2019** *10*, 16, 4587.

[13] A. Solanki, S. S. Lim, S. Mhaisalkar, T. C. Sum, *ACS Appl. Mater. Interfaces* **2019**, *11*, 25474.

[14] T. L. Bu, J. Li, W. C. Huang, W. X. Mao, F. Zheng, P. Q. Bi, X. T. Hao, J. Zhong, Y. B. Chengabe, F. Z. Huang, *J. Mater. Chem. A* **2019**, *7*, 6793.

[15] H. Y. Shu, J. X. Xia, H. Yang, J. S. Luo, Z. Q. Wan, H. A. Malik, F. Han, X. J. Yao, C. Y. Jia, *ACS Sustainable Chem. Eng.* **2020**, *8*, 10859.

[16] D. S. Lee, J. S. Yun, J. C. Kim, A. M. Soufiani, S. Chen, Y. Y. Cho, X. F. Deng, J. Seidel, S. Lim, S. J. Huang, A. W. Y. Ho-Baillie, *ACS Energy Lett.* **2018**, 3, 647.

[17] T. Wang, Y. P. Fu, L. R. Jin, S. B. Deng, D. X. Pan, L. Dong, S. Jin, L. B. Huang, J. *Am. Chem. Soc.* **2020**, *142*, 16254.

[18] Y Yang, C. Liu, A. Mahata, Mo Li, C. Roldán-Carmona, Y. Ding, Z. Arain, W. D. Xu, Y. H. Yang, P. A. Schouwink, A. Züttel, F. De Angelis, S. Y. Dai, M. K. Nazeeruddin, *Energy Environ. Sci*. **2020**, *13*, 3093.

[19] Y. Y. Zhang, S. Y. Jang, I. W. Hwang, Y. K. Jung, B. R. Lee, J. H. Kim, K. H. Kim, S. H. Park, *ACS Appl. Mater. Interfaces* **2020**, *12*, 24827.

[20] Y. N. Liu, J. J. Duan, J. K. Zhang, S. M. Huang, W. Ou-Yang, Q. Y. Bao, Z. Sun, X. H. Chen, *ACS Appl. Mater. Interfaces* **2020**, *12*, 771.

[21] S. Q. Li, L. N. Hu, C. X. Zhang, Y. K. Wu, Y. F. Liu, Q. J. Sun, Y. X. Cui, Y. Y. Hao, Y. C. Wu, *J. Mater. Chem. C* **2020**, *8*, 2425.

[22] C. L. Zhang, S. H. Wu, L. M. Tao, G. M. Arumugam, C. Liu, Z. Wang, S. S. Zhu, Yuzhao Yang, J. Lin, X. Y. Liu, R. E. I. Schropp, Y. H. Mai, *Adv. Energy Mater.* **2020**, *10*, 2002004.

[23] N. Lei, L. Pan, T. Ye, S.Chen, X. Wang, *Adv. Mater. Interfaces* **2020**, *7*, 2000197.

[24] R. J. E. Westbrook, W. D. Xu, X. X. Liang, T. Webb, T. M. Clarke, S. A. Haque*, J. Phys. Chem. Lett*. **2021**, *12*, 3312.

[25] Y. Y. Cho, H. D. Kim, J. H. Zheng, J. M. Bing, Y. Li, M. Zhang, M. A. Green, A. Wakamiya, S. J. Huang, H. Ohkita, A. W.Y. Ho-Baillie, *ACS Energy Lett.* **2021**, *6*, 925.

[26] K. Meng, X. Wang, Z. Li, Z. Liu, Z. Qiao, C. Wang, Y. Hu, S. Li, L. Cheng, Y. Zhai, G. Chen, *Energy Environ. Sci*., **2021**, 14, 2357.

[27] Y. Chen, Q. Meng, Y. Xiao, X. Zhang, J. Sun, C. Han, H. Gao, Y. Zhang, Y., and H. Yan, *ACS Appl.Mater. Interfaces* **2019** 11 (47), 44101.

[28] X. Li, D. Bi, C. Yi, J. D. Décoppet, J. Luo, S. M. Zakeeruddin, A. Hagfeldt, M. Grätzel, *Science*, **2016** 353(6294), 58-62.

[29] W. Chen, B. Han, Q. Hu, M. Gu, Y. Zhu, W. Yang, Y. Zhou, D. Luo, F. Liu, R. Cheng, R Zhu, S. P. Feng, A. B. Djurišić, T. P. Russell, Z. He, *Sci. Bull.* **2021** 66(10), 991-1002.

[30] S. Shao, M. Abdu-Aguye, L. Qiu, L.-H. Lai, J. Liu, S. Adjokatse, F. Jahani, M. E. Kamminga, G. H. ten Brink, T. T. M. Palstra, B. J. Kooi, J. C. Hummelen and M. Antonietta Loi, *Energy Environ. Sci.* **2016**, 9, 2444-2452.

[31] J. Yao, L. Yang, F. Cai, Y. Yan, R. S. Gurney, D. Liu and T. Wang, *Sustainable Energy Fuels*, **2018**, 2, 436-443.

[32] M. Jahandar, J. H. Heo, C. E. Song, K.-J. Kong, W. S. Shin, J.-C. Lee, S. H. Im and S.-J. Moon, *Nano Energy*, **2016**, 27, 330-339.

[33] Y. Huang, L. Li, Z. Liu, H. Jiao, Y. He, X. Wang, R. Zhu, D. Wang, J. Sun, Q. Chen, H. Zhou, *J. Mater. Chem. A* **2017**, 5, 8537.

[34] Z. Wu, M. Jiang, Z. Liu, A. Jamshaid, L. K. Ono, Y. Qi, *Adv. Energy Mater*. **2020** 10(10), 1903696.

[35] D. Yang, R. Yang, K. Wang, C. Wu, X. Zhu, J. Feng, X. Ren, G. Fang, S. Priya, S. Liu, *Nat. Commun.* **2018** 9(1), 1-11.

[36] W. Chen, Y. Zhou, G. Chen, Y. Wu, B. Tu, F. Liu, L. Huang, A. Ng, A. B. Djurišić, Z. He, *Adv. Energy Mater.* **2019**, 9. 1803872.

[37] Z. Liu, J. Chang, Z. Lin, L. Zhou, Z. Yang, D. Chen, C. Zhang, S. Liu, Y. Hao, *Adv. Energy Mater.* **2018**, 8, 1703432.

[38] W. A. Laban, L. Etgar, *Energy Environ. Sci.* **2013**, 6, 3249.

[39] F. Zhang, Q. Huang, J. Song, Y. Zhang, C. Ding, F. Liu, D. Liu, X. Li, H. Yasuda, K. Yoshida, J. Qu, S. Hayase, T. Toyoda, T. Minemoto, Q. Shen, *Sol. RRL* **2020**, 4, 1900243.

[40] K. Wang, Z. W. Jin, L. Liang, H. Bian, D. Bai, H. Wang, J. Zhang, Q. Wang, S. Liu, *Nat. Commun.* **2018**, 9, 4544.

[41] J. You, L. Meng, T. Song, T. Guo, Y. Yang, W. Chang, Z. Hong, H. Chen, H. Zhou, Q. Chen, Y. Liu, *Nat. Nanotechnol.* **2016**, 11, 75-81.

[42] M. Saliba, T. Matsui, J. Y. Seo, K. Domanski, J. P. C. Baena, M. K. Nazeeruddin, S. M. Zakeeruddin, W. Tress, A. Abate, A. Hagfedlt, M. Grätzel, *Energy Environ. Sci.* **2016**, 9, 1989-1997.

[43] G. Yang, Z. W. Ren, K. Liu, M. C. Qin, W. Y. Deng, H. K. Zhang, H. B. Wang, J. W. Liang, F. H. Ye, Q. Liang, H. Yin, Y. X. Chen, Y. L. Zhuang, S. Q. Li,, B. W. Gao, J. B. Wang, T. T. Shi, X. Wang, X. H. Lu, H. B. Wu, J. H. Hou, D. Y. Lei, S. K. So, Y. Yang G. J. Fang, G. Li, *Nature Photonics* **2021**, 15, 681-689.

[44] M. J. Kim, G. H. Kim, T. K. Lee, I. W. Choi, H. W. Choi, Y. H. Jo, Y. J. Yoon, J. W. Kim, J. Y. Lee, D. H. Huh, H. Lee, S. K. Kwak, J. Y. Kim, D. S. Kim, Joule **2019**, 3, 2179-2192.

[45] J. Li, L. J. Zuo, H. T. Wu, B. F. Niu, S. Q. Shan, G. Wu, H. Z. Chen, Adv. Funct. Mater. **2021**, *31*, 2104036.

[46] A. Rajagopal, K. Yao, A. K. Y. Jen, Adv. Mater. **2018**, *30*, 1800455.

[47] G. B. Wu, R. Liang, M. Z. Ge, G. X. Sun, Y. Zhang, G. C. Xing, Adv. Mater. **2022**, 34, 2105635.

[48] K. Yao, X. F. Wang, Y. X. Xu, F. Li, Nano Energy **2015**, 18, 165–175.

[49] M. Degani, Q. Z. An, M. Albaladejo-Siguan, Y. J. Hofstetter, C. S. Cho, F. Paulus, G. Grancini, Y. Vaynzof, *Sci. Adv.* **2021**, 7, eabj7930.

[50] F. B. Minussi, E. M. Bertoletti, S. P. Reis, J. F. Carvalho, E. B. Araujo, *Chem. Commun.* **2022**, Advance Article, DOI:10.1039/D1CC06642K.

[51] L. Xie, L. Chen, Z. Nan, H. Lin, T. Wang, D. Zhan, J. Yan, B. Mao, Z. Tian, *J. Am. Chem. Soc.* **2017**, 139, 3320-3323.

[52] D. Ju, T. Zhao, Y. Dang, G. Zhang, X. Hu, D. Cui, X. Tao, *J. Mater. Chem. A* **2017**, 5, 21919.

[53] J. Calabrese, N. L. Jones, R. L. Harlow, N. Herron, D. L. Thorn, Y. Wang, *J. Am. Chem. Soc.* **1991**, 113, 2328-2330.

[54] J. Song, Y. Dang, X. Liu, X. Tao, *CrystEngComm* **2020**, 22, 6310-6315.

[55] S. Ning, S. Zhang, J. Sun, C. Li, J. Zheng, Y. M. Khalifa, S. Zhou, J. Cao, Y. Wu, *ACS Appl. Mater. Interfaces* **2020**, 12, 43705-43713.

[56] H. Xu, Y. Wu, J. Cui, C. Ni, F. Xu, J. Cai, F. Hong, Z. Fang, W. Wang, J. Zhu, L.Wang, R. Xu, F. Xu, *Phys.Chem.Chem.Phys*. **2016**, 18, 18607-18613.

[57] V.M. Le Corre, E. A. Duijnstee, O. El Tambouli, J. M. Ball, H.J. Snaith, J. Lim, L. J. A. Koster, *ACS Energy Lett.* **2021**, 6, 1087-1094.

[58] H. Li, C. Li, S. Wen, C.Wang, G. Wang, C. Li, C. Wang, L. Huang, W. Dong, S. Ruan, *ACS Sustainable Chem. Eng.* **2018**, 6, 11295-11302.

[59] O. Almora, C. Aranda, E. Mas-Marzá, G.Garcia-Belmonte, *Appl. Phys. Lett.* **2016**, 109, 173903.

[60] A. Kahn, *Mater. Horiz*. **2016**, 3, 7-10.

[61] Q. D. Ou, C. Li, Q. K. Wang, Y. Q. Li, J. X. Tang, *Adv. Mater. Interfaces* **2017**, 4, 1600694.

[62] W. Peng, J. Yin, K. T. Ho, O. Ouellette, M. De Bastiani, B. Murali, O. El Tall, C. Shen, X. Miao, J. Pan, E. Alarousu, J. H. He, B. S. Ooi, O. F. Mohammed, E. Sargent, O. M. Bakr, *Nano Lett*. **2017**, 17, 4759-4767.

[63] J. Yang, Z. Yuan, X. Liu, S. Braun, Y. Li, J. Tang, F. Gao, C. Duan, M. Fahlman, Q. Bao, *ACS Appl. Mater. Interfaces* **2018**, 10, 16225-16230.

[64] M. Wang, B. Li, J. Yuan, F. Huang, G. Cao, J. Tian, *ACS Appl. Mater. Interfaces* **2018**, 10, 37005-37013.

[65] O. Fernandez-Delgado, P. S. Chandrasekhar,N. Cano-Sampaio, Z. C. Simon, A. R. Puente-Santiago, F. Liu, E. Castro, L. Echegoyen, *J. Mater. Chem. C* **2021**, 9, 10759-10767.

[66] A. Al-Ashouri, A. Magomedov, M. Roß, M. Jošt, M. Talaikis, G. Chistiakova, T. Bertram, J. A. Márquez, E. Köhnen, E. Kasparavičius, S. Levcenco, L. Gil-Escrig, C. J. Hages, R. Schlatmann, B. Rech, T. Malinauskas, T. Unold, C. A. Kaufmann, L. Korte, G. Niaura, V. Getautis, S. Albrecht, *Energy Environ. Sci.* **2019**, 12, 3356-3369.

PEAI treatment results in the formation of 2D PEA_2PbI_4 capping layer on 3D perovskite which passivates defects and increases hydrophobicity, but hinders electron collection. The ambient exposure downshifts the energy levels facilitating charge collection, improving both efficiency and stability. Energy level alignment with PEAI treatment is also affected by HTL/perovskite interface modification, which facilitates favorable alignment with PEA_2PbI_4.

*Yantao Wang,[1] Jingyang Lin,[1,2] Yanling He,[1] Yi Zhang,[1] Qiong Liang,[3] Fangzhou Liu,[1] Zhiwei Zhou,[4] Christopher C. S. Chan,[5] Gang Li,[3] Shien-Ping Feng,[4,6] Alan Man Ching Ng,[2] Kam Sing Wong,[5] Jasminka Popović,[7] Aleksandra B. Djurišić[1]**

Improvement in the Performance of Inverted 3D/2D Perovskite Solar Cells by Ambient Exposure